A Letters Journal Exploring the Frontiers of Physics

June 2012

EPL, **98** (2012) 58003 www.epljournal.org
doi: 10.1209/0295-5075/98/58003

Flow-induced channelization in a porous medium

A. Mahadevan[1], A. V. Orpe[2], A. Kudrolli[3] and L. Mahadevan[4(a)]

[1] *Woods Hole Oceanographic Institution - Woods Hole, MA 02543-1050, USA*
[2] *Chemical Engineering Division, National Chemical Laboratory - Pune 411008, India*
[3] *Department of Physics, Clark University - Worcester, MA 01610, USA*
[4] *School of Engineering and Applied Sciences, Department of Physics, Harvard University Cambridge, MA 02138, USA*

received 5 December 2011; accepted in final form 29 April 2012
published online 31 May 2012

PACS 81.05.Rm – Porous materials; granular materials
PACS 92.40.Gc – Erosion and sedimentation; sediment transport

Abstract – Flow through a saturated, granular, porous medium can lead to internal erosion, preferential flow enhancement, and the formation of channels within the bulk of the medium. We examine this phenomenon using a combination of experimental observations, continuum theory and numerical simulations in a minimal setting. Our experiments are carried out by forcing water through a Hele-Shaw cell packed with bidisperse grains. When the local flow-induced stress exceeds a critical threshold, the smaller grains are dislodged and transported. This changes the porosity of the medium, thence, the local hydraulic conductivity, and leads to the development of erosional channels. Erosion is ultimately arrested due to the drop in the mean pressure gradient, while most of the flow occurs through the channels. We describe this using a minimal multiphase description of erosion where the volume fraction of the fluid, mobile, and immobile, grains change in space and time. Numerical solutions of the resulting initial boundary value problem yield results for the dynamics and morphology that are in qualitative agreement with our experiments. In addition to providing a basis for channelization in porous media, our study highlights how heterogeneity in porous media may arise from flow as a function of the erosion threshold.

The dynamics of fluid flow through porous continua is relevant over many orders of magnitude in length scale with applications that range from large-scale flow through fractured rock in aquifers and oil reservoirs to small-scale flows in natural and artificially engineered systems [1,2]. In all these cases, flows are characterized by large variations in hydraulic conductivity of the medium. This heterogeneity is usually ascribed to processes associated with the formation and consolidation of the porous medium via the agglomeration of grains (in geology) and cells (in biology). But heterogeneity and channelization may also arise due to selective erosion of material in non-cohesive porous media. Indeed, flow-induced erosion, on the surface of, and, in the bulk of porous media has been implicated in the formation of patterns on planetary [3,4], littoral [5], river-bank [6] and laboratory [7,8] scales that involve both unconsolidated and consolidated media [9–13]. Dissolution and liquefaction can also arise from reactive instabilities as seen in melt migration [14,15] and cave formation [16]. Here we explore the purely physical erosive instabilities occurring in the bulk of fluid saturated materials which can lead to internal channelization via the dynamic coupling of flow and changes in hydraulic conductivity.

We start by describing some experiments that demonstrate how erosion and channelization can occur in a saturated porous medium (see `Movie1_1.mov` in the supplementary information). The experiments were carried out in a fluid-saturated porous medium confined to a vertical quasi–two-dimensional chamber based on a Hele-Shaw cell filled with bidisperse mixture of glass beads as shown in fig. 1(A). The width between the walls of the apparatus is such that gravity is unimportant owing to the formation of arches between walls [17]. As our porous medium, we use a mixture of beads; 60% of the initial volume has large beads (diameter $d_1 = 4 \pm 0.1$ mm) and 24% has small beads ($d_2 = 0.7 \pm 0.1$ mm). The width of the chamber, chosen to be $1.2 \times d_1$, enables visualization of the porosity pattern, and allows the larger beads to be rearranged locally without being transported by the flow, while the smaller beads can be dislodged and transported through the matrix of large beads. Since only the smaller beads can be eroded, we scale the porosity by the maximum attainable absolute porosity, 0.4, so that the scaled porosity or liquid volume fraction $\phi_l \in [0, 1]$. To observe

(a) E-mail: `lm@seas.harvard.edu`

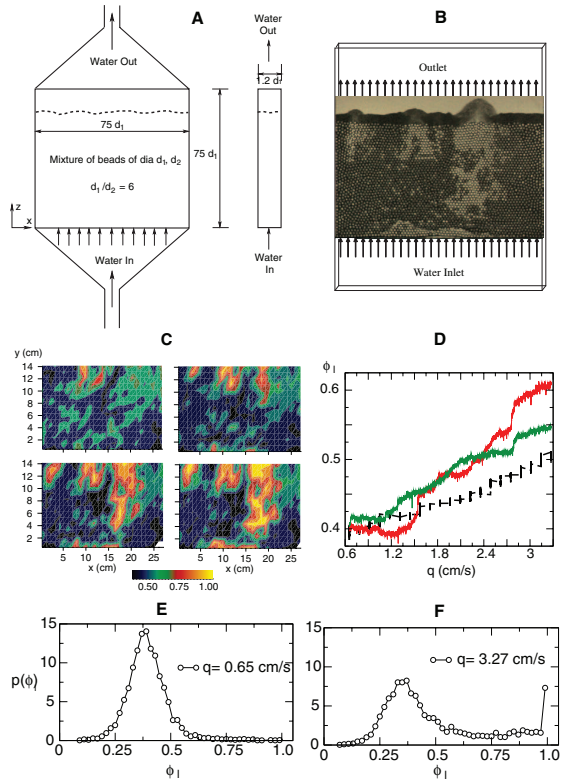

Fig. 1: (Color online) Experiments. (A) Schematic of the experimental setup showing face-on and sectional views. (B) An instantaneous snapshot showing the spatially varying porosity generated by the flow. Light color indicates high porosity where the small beads have been removed by erosion. Small beads transported out of the porous medium are seen to pile up at the interface between the porous bed and clear water. (C) Maps of the scaled porosity ϕ_l (absolute porosity normalized by the maximum attainable absolute porosity) for specific discharge rates $q = 0.65$, 1.3, 1.96 and 2.62 cm/s after the system has reached a steady state. (D) Domain-averaged ϕ_l is plotted as a function of specific discharge q as it is ramped up over 3 hours (red and green curves) or stepped incrementally every 10 min intervals (black points) so as to achieve a near steady state for each flow rate. Histogram or probability distribution of relative porosity $p(\phi_l)$ shown after steady state is achieved for a specific discharge rate (E) $q = 0.65$ cm/s and (F) $q = 3.27$ cm/s. For low discharge rates ($q = 0.65$ cm/s in (E)), the peak in $p(\phi_l)$ is slightly broadened with respect to the initial condition, but remains at the initialized value of $\phi_l = 0.4$. At higher discharge rates ($q = 3.27$ cm/s in (F)) the distribution broadens further and a second peak that represents completely eroded channels is developed at $\phi_l = 1$.

the evolution of the porosity induced by fluid flow, we use a back-lighting technique and an intensity-density calibration that allows us to obtain the volume fraction of liquid (void fraction) or porosity as a function of space and time at a grid resolution of $d_1 \times d_1$ ($4 \times 4\,\mathrm{mm}^2$) in 2 dimensions (fig. 1(C)).

We control the inlet flow rate Q, which is applied uniformly to the lower boundary of the experimental domain to provide a uniform specific discharge $q = Q/A$ over the cross-sectional area A. Since the sudden imposition of a large flow rate (and pressure gradient) can cause the entire medium to fluidize, we gradually ramp up the flow rate at the inlet from 500 to 2500 cm^3/min over 3 hours so that q increases from 0.65 and 3.27 cm/s. The increase in flow rate is carried out smoothly, as well as in steps of 0.13 cm/s over time intervals of 600 s to allow for equilibration, but the behavior is qualitatively the same in both cases (fig. 1(D)). The outlet at the upper boundary is maintained at atmospheric pressure. By measuring the pressure at the inlet, we determined the average pressure gradient and found that it increases linearly with the flow rate for a constant porosity, confirming that the flow within the porous medium obeys Darcy's law even after channels are formed. With each increment in the flow rate, erosion occurs for a few minutes before stopping. As a consequence, the porous medium which is initially fairly uniform in porosity, becomes increasingly heterogeneous as the flow rate is increased, as erosion generates regions of enhanced porosity that connect to form channels with high conductivity (fig. 1(B), (C)). The erosion patterns coarsen with time and eventually, just a few channels preferentially conduct most of the flow.

Mechanistically, we observe that as the flow rate is gradually increased, the flow-induced stress, *i.e.*, the magnitude of the local pressure gradient, can exceed the local threshold required to dislodge and mobilize particles that are held in place by the confinement pressure due to particle packing between the walls. For our bidisperse medium, the process involves the dislodgment and movement of the smaller grains from the interstices between the larger grains. This leads to a local increase in the hydraulic conductivity and a readjustment of the flow. As the material erodes and porosity increases, the pressure gradient drops below the critical erosive stress threshold and erosion stops. Thus, for every increment in the flow rate, the pressure gradient is raised above the threshold and leads to further erosion for a short while before it stops. For a given flow rate, the porosity evolves in space and time until it reaches a steady state that is a function of the initial heterogeneity in the porosity of the medium. Although deposition can act to mitigate the erosion patterns by decreasing the porosity and the hydraulic conductivity downstream, this effect is strongly dependent on whether the outflow region serves to sieve the mobile particles or trap them; in our system, this effect is negligible.

The spatial pattern of porosity can vary significantly from one experiment to another due to the slight inhomogeneity in the initial conditions of the medium. However, in all cases, the basic phenomenon is robust; preferential erosion, coupled to flow through positive feedback leads to the formation of channels of highly variable conductivity from a relatively uniform porous medium. The average porosity over the region is observed to

increase linearly with flow rate for scaled porosity in the range 0.4–0.6 as shown in fig. 1(C), (D). The distribution (pdf) in porosity values over the region is shown in fig. 1(E), (F) for small and large flow rates, respectively. Initially, the distribution is broadly peaked at $\phi_l \sim 0.4$ corresponding to 60% large and 24% small beads. As the flow increases, a second peak develops at $\phi_l \sim 1$ corresponding to regions containing only large beads where complete erosion of the finer beads has occurred, a process that is concomitant with channelization.

Motivated by these qualitative observations, we now turn to a continuum theory for the dynamical evolution of channels via flow-induced erosion within a saturated porous medium. Our theory for the active co-evolution of the phases in a porous medium is qualitatively different from the single phase diffusive models for the evolution of free surfaces by aggregation and erosion [6,7], but has some superficial similarities to multiphase bulk theories for particle production and migration in porous media [11–13], and geophysical theories for multiple reactive fluids interacting with each other [14,16] in that it accounts for multiple phases. Indeed, we combine features of these previous models in considering the fluid-induced erosion and deposition processes acting in the bulk of a solid skeleton. To correctly account for the onset of erosion and its evolution as observed in the quasi–two-dimensional bidisperse granular medium, we propose a multiphase theory that involves fluid, granular and immobile phases interacting with each other. However, we do not consider the microscopic mechanisms in detail and instead use simple symmetry-based arguments for the form of the interaction between these phases, in the spirit of effective theories in condensed-matter physics [18].

To enable a continuum field description of the process, we use a representative volume much larger than the grain/pore size with $\phi_s(x,y,z,t)$ the volume fraction of the immobile solid phase, $\phi_g(x,y,z,t)$, the volume fraction of the granular mobile phase, and $\phi_l(x,y,z,t)$, the liquid volume fraction in the medium so that $\phi_s + \phi_g + \phi_l = 1$. Volume conservation for the individual phases (each assumed to be incompressible) implies that

$$\partial_t \phi_s = -e + d, \tag{1}$$

$$\partial_t \phi_g = +e - d - \nabla\cdot(\phi_g \mathbf{u}_g), \tag{2}$$

$$\partial_t \phi_l = -\partial_t(\phi_s + \phi_g) = -\nabla\cdot(\phi_l \mathbf{u}_l), \tag{3}$$

where the erosion rate, e, is the rate of transformation of the immobile phase to mobile phase, d, is the rate of deposition (or conversion of mobile phase to immobile phase), and $\mathbf{u}_g$ and $\mathbf{u}_l$ denote the velocity of the granular and liquid phases, respectively. We note that adding eqs. (1)–(3) yields the global continuity equation

$$\nabla\cdot(\phi_g \mathbf{u}_g + \phi_l \mathbf{u}_l) = 0. \tag{4}$$

For simplicity, we will assume that $\mathbf{u}_g = \mathbf{u}_l = \mathbf{u}$, *i.e.*, the granular and liquid phases have the same velocity and the effects of inertia and body forces associated with sedimentation are negligible, a reasonable approximation for slow flows of nearly jammed grains. Then the continuity equation reduces to $\nabla\cdot(\phi\mathbf{u}) = 0$, where $\phi \equiv \phi_g + \phi_l$. In a saturated porous medium, erosion of ϕ_s can occur only when the fluid-induced stress exceeds a critical threshold σ that is determined by the confinement pressure induced by the packing of the grains. Then we may write the local erosion rate as

$$e = k_e \phi_s \left((\gamma^{-1}\nabla p)^2 - \sigma\right) \geqslant 0, \tag{5}$$

where $k_e = q_0/L$ is a characteristic rate related to the specific discharge q_0 and a system length L (determined experimentally), and $\gamma = q_0/D_0$ the ratio of the characteristic specific discharge ($q_0 = 10^{-2}\,\mathrm{m/s}$) to characteristic hydraulic conductivity ($D_0 = 10^{-6}\,\mathrm{m^3\,s\,kg^{-1}}$), is used to normalize the pressure gradient. The form of e follows from considerations of symmetry: a hydrostatic pressure p cannot lead to erosion, but a gradient can. However, the sign of the gradient is not important, so that we have chosen the simplest analytic dependence consistent with this symmetry (using the asymptotically correct, but non-analytic form $|\nabla p|$ instead of $(\nabla p)^2$ yields qualitatively similar results). We assume that the critical threshold for erosion σ is a regionally averaged function of the solid volume fraction ϕ_s given by $\overline{\phi}_s = V^{-1}\int_V \phi_s \mathrm{d}v$, since elastic stresses induced by flow are felt over a scale V compared to a few grain volumes. Although the form of σ is difficult to gauge from our experiments, we use the function $\sigma = 2(\tanh(2\pi(\overline{\phi}_s - 0.6)) + 1)$, where $0 \leqslant \overline{\phi}_s \leqslant 1$ which mimics the sharp dependence of the failure stress σ on the solid volume fraction.

A simple model for d, the rate at which the mobile granular material is converted back to the immobile solid phase, is given by

$$d = k_d(\phi_s - \phi_s^*)\,\phi_g \geqslant 0. \tag{6}$$

The form of the deposition, with rate $k_d = q_0/L$ (which can be determined experimentally), is based on a binary collision picture —mobile grains will come to rest only if they interact with immobile grains; hence the dependence on ϕ_s with a threshold ϕ_s^*, which we take to be 0.

In the porous medium, we assume that the volumetric flow rate per unit cross-sectional area, *i.e.*, the specific discharge $\mathbf{q} \equiv \mathbf{u}(\phi_l + \phi_g)$, is given by Darcy's law[1]

$$\mathbf{q} \equiv \mathbf{u}\phi = -D(\phi)\nabla p, \text{ where } D = \frac{\phi^3\, l_p^2}{A\mu\,(1-\phi^2)}. \tag{7}$$

Here, $D(\phi)$, the hydraulic conductivity, is assumed to follow the Carman-Kozeny relation [2] and is in general a nonlinear function of the porosity $\phi = \phi_l + \phi_g$. Here

[1]This can be generalized to a Brinkman-like equation if necessary in regions of high porosity.

l_p is the nominal pore size (which scales with the grain diameter), μ is the dynamic viscosity of the interstitial fluid, and the dimensionless constant $A = 180$ for spherical grains [2]. For $l_p = 1\,\mathrm{mm}$, $\mu = 10^{-3}\,\mathrm{kg\,m^{-1}\,s^{-1}}$, D ranges from 0.6×10^{-7} to $1.6 \times 10^{-5}\,\mathrm{m^3\,s\,kg^{-1}}$ for ϕ between 0.1 and 0.9.

We use the domain size, $L = 1\,\mathrm{m}$, specific discharge $q_0 = 1\,\mathrm{cm/s}$, and time scale $T = L/q_0$ to make the problem dimensionless, so that the dimensionless parameters in the problem include the thresholds for erosion and deposition σ and ϕ_s^* as well as the ratio of deposition to erosion rates $\Pi_1 = \frac{k_d}{k_e}$, and the ratio of advection to erosion rate $\Pi_2 = \frac{q_0}{k_e L}$. Our choice of k_e and k_d implies that $\Pi_1 = \Pi_2 = 1$. We solve eqs. (1)–(7) numerically in 2 dimensions (x, y) using a finite volume method. In the x-direction, we use periodic boundary conditions at $x = 0$ and $x = L_x$, with a square domain of dimension $L_x = 0.32, L_y = 0.32$ and a uniform grid resolution $\Delta = 0.05$. Prescribing the inlet pressure instead of the inlet discharge leads to either no erosion (if $(\gamma^{-1}\nabla p)^2 < \sigma$) or catastrophic erosion if the pressure gradients are larger than the erosion threshold. Thus, we prescribe a constant scaled specific discharge $q_0 = 1$ at the inflow boundary $y = 0$, while at the outflow boundary $y = L_y$ we set pressure $p = 0$ (atmospheric pressure). The pressure is determined by iteratively solving the Poisson equation $\nabla(D(\phi)\nabla p) = 0$ obtained by substituting (7) into (4), then calculating the erosion rate e and the deposition rate d, and finally evolving eqs. (1)–(3) to update the volume fraction of the phases ϕ_s, ϕ_g, ϕ_l from one time step to the next, with scaled time step $\Delta t = 10^{-4}$. Starting with an initial volume fraction of mobile grains $\phi_g = 0$ throughout the domain, and a mean liquid volume fraction $\phi_l = 0.2$ with an additive white Gaussian noise (standard deviation $sd = \sqrt{\langle\phi_l^2\rangle - \langle\phi_l\rangle^2}^{1/2} = 0.01$) that describes the weak heterogeneity in σ, we allow the system to evolve until it reaches a quasi-steady state. The non-local form of the erosion threshold σ is based on $\overline{\phi}_s$, the weighted spatial average of ϕ_s, which is calculated numerically as $\overline{\phi}_s(i,j) = 0.2\phi_s(i,j) + 0.1\phi_s$ $(i \pm 1, j \pm 1)$. Averaging over the 8 surrounding neighbors of a grid point amounts to a radius of influence of the stress that extends a few grain diameters, in contrast to using a local value of ϕ_s that would lead to runaway erosion at individual grid cells.

In fig. 2(A), (B) we show two snapshots of the porous medium as it erodes and channelizes (see `Movie2.mov` in the supplementary information). This process involves positive feedback: flow is enhanced through the regions of low solid fraction (high hydraulic conductivity), while regions with a higher solid fraction and lower hydraulic conductivity are circumvented by the flow. Indeed, in fig. 2(C), (D) we see the interplay between the heterogeneity in the erosion threshold σ and the squared pressure gradient $(\gamma^{-1}\nabla p)^2$. The material is transformed from solid to mobile phase where $(\gamma^{-1}\nabla p)^2 > \sigma$ and transported by the flow, reducing $\overline{\phi}_s$, lowering σ, and augmenting erosion. The channelization leads to enhanced flow through regions of high hydraulic conductivity at the expense of other regions (fig. 2(E)) even as the total flow rate remains the same. In fig. 2(F), we provide a global view of the process. As erosion progresses, the average porosity and hydraulic conductivity over the entire domain increases. The pressure gradient required to sustain the same flow rate drops

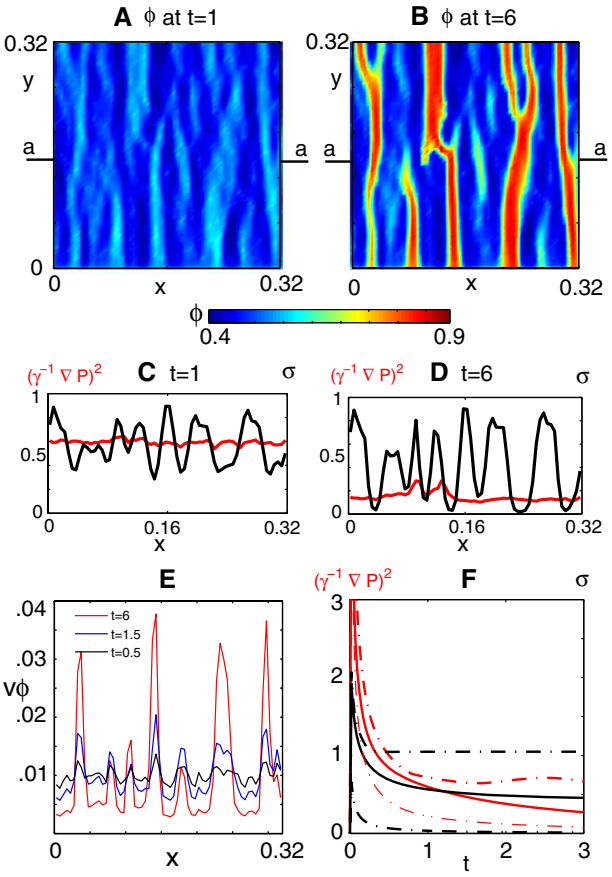

Fig. 2: (Color online) Numerical solution to eqs. (1)–(7) with a steady specific discharge $q = q_0$ prescribed at the lower boundary $y = 0$, and constant pressure at the upper boundary $y = 0.32$. (A) Spatial distribution of porosity ϕ at $t = 1$ and (B) at $t = 6$. (C) $(\gamma^{-1}\nabla P)^2$ (red) and σ (black) are plotted along a–a (at $y = 0.16$) at $t = 1$ and (D) at $t = 6$ corresponding to the panels above. Erosion occurs where $(\gamma^{-1}\nabla P)^2 > \sigma$. At early times, this occurs at several locations. As erosion progresses, the pressure gradient drops, heterogeneity in σ increases, and erosion is limited only to the channels. (E) The flux in the y-direction, $v(\phi_g + \phi_l)$ plotted at section a–a at $t = 0.5$ (black), $t = 1.5$ (red), and at $t = 6$ (blue). As the flux increases in eroded regions, it decreases in non-channelized regions. (F) Domain-averaged time evolution of the scaled pressure gradient squared (solid red line) and erosion threshold (solid black line), with one standard deviation plus or minus (dash-dotted lines) indicated. Initially, the area-averaged $(\gamma^{-1}\nabla p)^2 > \sigma$, but as erosion progresses, the pressure gradient decreases, $(\gamma^{-1}\nabla p)^2 < \sigma$, and erosion no longer occurs, except in a few places.

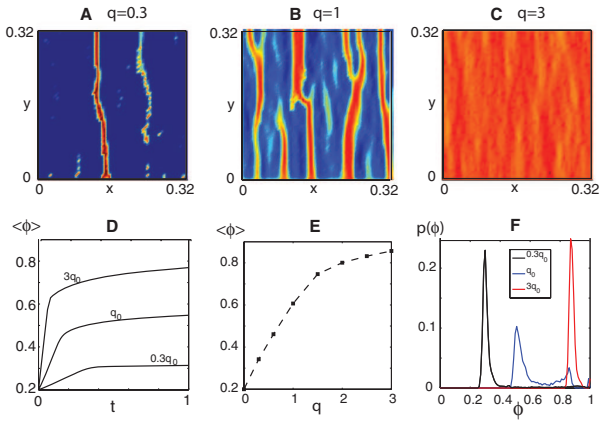

Fig. 3: (Color online) The final distribution of porosity ϕ at $t=6$ depending on the specific discharge q (scaled by q_0) specified at $y=0$; (A) $q=0.3$, (B) $q=1$, (C) $q=3$. (D) For each q, the average porosity increases with time, until as steady state is achieved. (E) The final porosity (at $t=6$) is a function of q at the inlet. (F) Histograms of the porosity distribution for $q=0.3$, 1 and 3 shows bimodality and a peak at $\phi=1$ due to channelization.

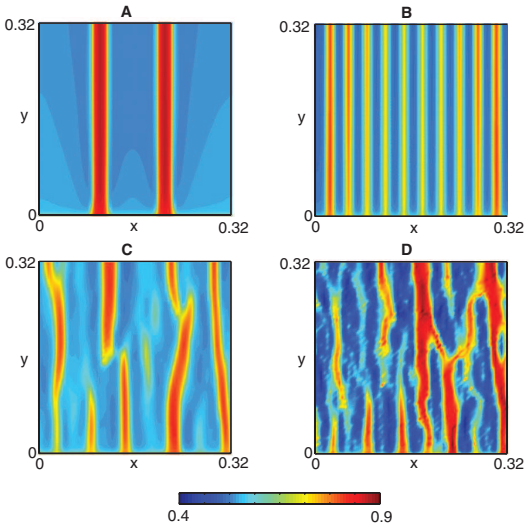

Fig. 4: (Color online) The final distribution of porosity (at $t=6$) is shown to be sensitive to the initial heterogeneity in σ arising from ϕ_s. The upper row shows the porosity distribution resulting when the initial distribution of ϕ_s is set to 0.8 everywhere, except in specific places where it is decreased by 1% from the uniform background value (A) along two lines, and (B) along 10 lines, each being one grid cell wide. In the lower row, the standard deviation (sd) in the initial perturbation to ϕ_s is varied from its previous value of $sd=0.01$. (C) $sd=0.001$. (D) $sd=0.03$.

until it falls below the threshold for erosion almost everywhere and the system asymptotically approaches a steady state.

To understand how this steady state depends on the dimensionless parameters, we first vary the scaled specific discharge at the inlet q/q_0. When $q<q_c$, a critical scaled flow rate that depends on the initial porosity distribution in the medium, no erosion or channelization occurs, because the pressure gradient is everywhere smaller than the erosion threshold. For $q=q_c$, a single narrow channel and secondary partial channel are formed as shown in fig. 3(A). As q is increased further, the number of channels as well as the width of channels increases (fig. 3(B)); for even higher flow rates, the entire medium begins to erode away as shown in fig. 3(C). In all cases, the porosity increases with time after initiation of the flow (fig. 3(D)), linearly at first, and then slowly approaching a steady-state value that depends on the inlet specific discharge. Much like the experiments, the average porosity of the medium is a function of the inflow q (fig. 3(E)). Histograms of the porosity for varying inflow rates are shown in fig. 3(F); the case $q=1$, produces the most bimodal porosity due to channelization.

Varying the erosion and deposition rates also leads to variations in the erosion patterns. A 10-fold increase in erosion rate k_e ($\Pi_1=0.1$), leads to a faster evolution of channels. Increasing k_d 100-fold so that $\Pi_1=100$ increases the deposition rate and causes blockages that leads to termination and re-initiation of channels. In this model, deposition remains small even when $k_d=k_e$, because $\phi_g \ll \phi_l$ and a significant (100-fold) increase in k_d is needed before we begin to see the effects of deposition. The average number or size of channels does not change in either case relative to when $\Pi_1=1$ (corresponding to fig. 2(B)).

A question that naturally arises is the mechanism for the selection of channel spacing and width when fluid flows through a nominally homogeneous porous medium. We find that the spacing and width of channels is insensitive to the domain size; doubling the model domain size does not change the picture. The natural length scales in the problem are the system size L, the nominal pore size l_p, which evolves with time, but remains a microscopic length, and the length scales $q_0/k_e, q_0/k_d$; the latter control the dynamical evolution of the channels but not their final state. What remains is the role of the threshold for erosion σ. The onset of channelization is strongly influenced by fluctuations in the porosity (and thus the fragility) of the medium, and stability analysis of the uniform base state predicts that channels form at locations where σ is smallest initially. Thus, for the same inlet specific discharge, the size and number of channels are a function of $\sigma(x,y,0)$. In fig. 4(A) we show that for a given inlet specific discharge, if $\sigma(x,y,0)\equiv f(x)$ has a single minimum, a single channel forms and grows until the pressure gradient falls below the erosion threshold, while in fig. 4(B), we see that if $\sigma(x,y,0)$ has multiple minima, multiple channels form. Of course, it is not sufficient to consider the mean value of the threshold; instead one must account for the complete probability distribution of

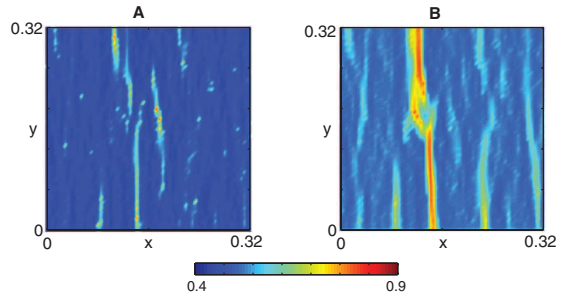

Fig. 5: (Color online) The evolution of the porosity is sensitive to the functional form of the erosion threshold σ. Here the final distribution of porosity ϕ is shown for other choices of σ. (A) $\sigma = \overline{\phi}_s$, (B) $\sigma = \overline{\phi}_s^2$. These results can be compared with fig. 1, where $\sigma = 0.5(\tanh(2\pi(\overline{\phi}_s - 0.6)) + 1)$ (subtracting 0.6 instead of 0.5 provides a slight asymmetry to the tanh profile).

the erosion threshold. For our simple Gaussian model of disorder, if the variance in the threshold for erosion (or equivalently the porosity fluctuations) is also changed, this leads to variations in the patterns as well. In fig. 4(C), (D), we show that an increase in the standard deviation of the initial white noise leads to greater heterogeneity in the channel number and spacing. These considerations change qualitatively if there are body forces such as gravity, which would lead to the introduction of a new length scale due to the competition between flow-induced stresses and gravity.

Finally, we consider the functional form of the erosion threshold $\sigma(\overline{\phi}_s)$. In fig. 5, we see that as σ varies more strongly with $\overline{\phi}_s$, the final morphology of the erosion patterns becomes more variable; indeed the form of the erosion threshold function, and its initial, possibly heterogeneous spatial distribution are crucial in determining the growth and form of the channels.

Our model qualitatively captures the basic features of our physical experiments: below a critical flow rate, little or no erosion occurs. Above this threshold, the porous medium starts to erode heterogeneously at locations where the critical threshold is lowest; positive feedback then enhances erosion locally in other regions leading to oriented regions of higher porosity, *i.e.*, channels which can branch, start or stop in the medium. For a given flow rate, the pressure gradient and erosion rate decay with time as channels form. Consistent with this, we find an increase in the average porosity of the region for higher flow rates. The strong dependence of the channelization patterns on the heterogeneity of the initial porosity is a feature of both our experiments and our numerical simulations. Indeed this is why we cannot predict the wavelength of the channelization patterns, which are instead determined by a combination of the prescribed flow rate and the initial distribution of variations in porosity. Taken together, our qualitative experiments and continuum model allow us to describe flow through porous media by accounting for erosion, deposition, and dynamic permeability changes, which lead to channelization. A natural next step is a quantitative comparison with experiments and a microscopic derivation of the model equations that we have proposed here.

* * *

We thank NSF (grant EAR-1131393, AM), DOE (grant DE-FG0202ER15367, AK), Harvard-NSF MRSEC (LM) and the MacArthur Foundation (LM) for partial support, and Andrew Fowler for comments on an earlier draft and Jim Rice for discussions.

REFERENCES

[1] Scheidegger A. E., *The Physics of Flow through Porous Media* (Macmillan Company, New York) 1960.
[2] Bear J., *Dynamics of Fluids in Porous Media* (Dover, New York) 1988.
[3] Harbor J., Hallet B. and Raymond C., *Nature*, **333** (1988) 347.
[4] Malin M. C. and Edgett K., *Science*, **288** (2000) 2330.
[5] Hughes Z. J., FitzGerald D. M. *et al.*, *Geophys. Res. Lett.*, **36** (2009) L03602.
[6] Rodriguez-Iturbe I. and Rinaldo A., *Fractal River Basins* (Cambridge University Press) 1997.
[7] Schorghofer N., Jensen B., Kudrolli A. and Rothman D. H., *J. Fluid Mech.*, **503** (2004) 357.
[8] Daerr A., Lee P., Lanuza J. and Clement E., *Phys. Rev. E*, **67** (2003) 06520.
[9] Cerasi P. and Mills P., *Water Resour. Res.*, **24** (1998) 1659.
[10] Jain A. K. and Juanes R., *Phys. Rev. E*, **58** (2009) 6051; *J. Geophys. Res.*, **114** (2009) B08101.
[11] Vardoulakis I., Stavropoulou M. and Papanastasiou P., *Transp. Porous Media*, **22** (1996) 225.
[12] McDowell-Boyer L. M., Hunt J. R. and Sitar N., *Water Resour. Res.*, **22** (1986) 1901.
[13] Khilar K. C. and Fogler H. S., *Migration of Fines in Porous Media, Series: Theory and Applications of Transport in Porous Media* (Kluwer Academic Publishers) 1998.
[14] McKenzie D., *J. Petrol.*, **25** (1984) 713.
[15] Spiegelman M., *J. Fluid Mech.*, **247** (1993) 17.
[16] Szymczak P. and Ladd A. J., *Geophys. Res. Lett.*, **38** (2011) L07403.
[17] Sperl M., *Granular Matter*, **8** (2006) 59.
[18] Chaikin P. M. and Lubensky T. C., *Principles of Condensed Matter Physics* (Cambridge University Press) 1995.